Oxidation of Metals, Vol. 9, No. 6, 1975

Na_2SO_4- and NaCl-Induced Hot Corrosion of Six Nickel-Base Superalloys*

Y. Bourhis† and C. St. John†

Received June 11, 1975

The short-time hot-corrosion behavior of six industrial nickel-base superalloys was investigated with static deposits of Na_2SO_4 or NaCl or both in still air. The oxidation kinetics and scale morphologies were measured with traditional laboratory techniques—thermobalance, metallography, electron microprobe, and x-ray analyses. Susceptibility to hot corrosion was found to be correlated to the type of scale produced during simple oxidation. Alloys forming an Al_2O_3 scale were found to be susceptible to Na_2SO_4 deposits, independent of their chromium content. The quantity of Na_2SO_4 deposit dictated the nature of the attack and, under certain conditions, the refractory element alloy additions appeared to play an essential role. Alloys containing Cr_2O_3 or TiO_2 in the simple oxidation scale proved to be sensitive to NaCl attack. Again, the severity of the attack within the susceptible alloy group was not related to the chromium or titanium content. Although less intensive than the Na_2SO_4-induced hot corrosion, NaCl contaminations provoked extensive spalling. All of the hot-corrosion types encountered in this study were interpreted in the light of existing theories.

KEY WORDS: hot corrosion; Na_2SO_4; NaCl; nickel-base superalloys.

INTRODUCTION

The accelerated oxidation or hot corrosion of turbine blading due to the presence of fuel and airborne contaminants is considered to be one of the principal restrictions in gas turbine design and operation. A considerable amount of research and development has been devoted to this problem during

*Supported by the Délégation Générale à la Recherche Scientifique et Technique.

†Centre des Matérieux de l'Ecole Nationale Supérieure des Mines de Paris, Corbeil-Essonnes, France.

the last few years. Generally speaking, the experimental approaches tend to fall into two categories—mechanism-oriented studies that allow precise control of experimental parameters under unrealistic conditions or alloy development studies under simulated gas turbine conditions with limited parameter control. One might add a third class of test where rapidity and low cost are obtained at the expense of both parameter control and realism.

What appears to be necessary in order to exploit effectively the advantages of each of the first two approaches is to establish an intertest correlation between the respective results. In this way, the unnecessary development of mechanistic theories that do not have a counterpart under closely simulated operating conditions may be avoided.

The experimental results presented in this paper were obtained by the traditional mechanistic means, that is, thermobalance, metallography, electron microprobe, and x-ray analyses. The hot-corrosion conditions were not realistic. The results of a parallel burner rig investigation using identical alloys will be discussed in another paper and compared with those of this mechanistic study. The object of the parallel studies is the establishment of an intertest correlation of the sort mentioned above. The alloys and hot-corrosion conditions treated in this paper pertain to aviation gas turbines.

MATERIALS AND TESTING

Alloys

The commercial nickel-base alloys examined in this study and their chemical analyses are shown in Table I. All the alloys are cast except for U710, which is forged.

The alloys were given their standard heat treatment: IN100 and IN713LC, 2 hr at 870°C in argon, air-cooled; MARM002, 16 hr at 870°C in argon, air-cooled; IN738, 2 hr at 1120°C followed by 24 hr at 845°C in argon, air-cooled; IN597, 4 hr at 1150°C followed by 16 hr at 850°C in argon,

Table I. Chemical Analyses of the Alloys in Weight Percent

Alloy	Ni	Cr	Co	Mo	W	Fe	Al	Ti	Other	C
IN100	61.7	9.8	13.9	2.75	—	0.2	5.85	4.8	0.9 V	0.15
MARM002	58.6	9	9.85	—	10.9	0.3	5.5	1.7	2.55 Ta, 1.44 Hf	0.16
IN713LC	75.4	11.4	—	3.95	—	—	6.3	0.8	2.1 Nb	0.08
IN738	61.8	15.6	8.5	1.75	2.5	0.12	3.5	3.5	2.62 (Nb + Ta)	0.17
U710	60.7	18	12.8	1.6	—	0.13	2.4	4.3	—	0.09
IN597	48.3	23.9	18.5	1.4	—	0.43	2.25	5.2	—	0.05

air-cooled; U710, 4 hr at 1175°C followed by 4 hr at 1080°C, 24 hr at 845°C, and 16 hr at 760°C in argon, air-cooled.

Hot-Corrosion Testing

The hot-corrosion tests were carried out with Na_2SO_4- or NaCl-contaminated specimens or both in still air. Simple oxidation tests without contamination were also done for comparison. The specimens were disk-shaped (approximately 10 mm in diameter by 2 mm thick) with about 2 cm^2 of surface area. Prior to testing, the flat surfaces of the specimens were polished to 800 grit, cleaned ultrasonically in a distilled water–Teepol solution, and rinsed in distilled water.

The test temperature generally employed was 900°C since previous burner rig studies[1,2] suggest that this temperature is close to that which provokes the greatest attack with Na_2SO_4. However, other temperatures within the range 850–1000°C were also examined, but less systematically.

Two test procedures were used to measure the hot-corrosion kinetics. The first procedure exploited a microthermobalance apparatus (a SETARAM instrument with a precision of 0.01 mg) in conjunction with precontaminated specimens. The precontamination was effected by dipping the specimens into an aqueous solution of the salt and drying at approximately 150°C. The salt concentration of the aqueous solution was adjusted so as to provide a surface salt deposit that could be varied between 0.5 and 2 mg/cm^2. The microthermobalance technique, while yielding extensive data on the kinetics of hot corrosion, suffers from the static nature of the contamination procedure.

The second technique employed in this study complemented the first in that the contamination was renewed *in situ* during the hot-corrosion test. The recontamination was carried out periodically by momentarily dipping the specimen into a molten salt bath. This procedure produced contaminations that were very heavy (about 5 mg/cm^2) and, being simply a furnace experiment, yielded only total weight gains at the end of the tests. The furnace test also facilitated thermal shock experiments and tests of long duration.

Structural and Chemical Analysis

The scale dimensions and morphology were established with standard metallographic procedures. The photomicrographs illustrating this paper were taken on unetched metallographic sections.

The composition and structures of the scale products were determined, whenever possible, by combining the results of x-ray (Debye–Scherrer and spectrographic) and electron microprobe (M.S. 46 CAMECA) analyses.

Table II. Scale Compositions for the Cr_2O_3-Forming Alloys Oxidized at 1000°C for 24 hr

				TiO_2–Cr_2O_3	TiO_2–Cr_2O_3–TiO_x	Al_2O_3
Alloy	Cr	Al	Ti	Al_2O_3–Ti(CN)	Al_2O_3–Ti(CN)	
IN597	24	2.3	5.2	100%		
U710	18	2.4	4.3	50%	50%	
IN738	16	3.5	3.5	95%		5%

The electron microprobe results were corrected for absorption and interelement interactions with the Tong correction routine.[3]

RESULTS

Oxidation Without Contamination

The simple oxidation experiments, that is, oxidation without contamination in still air, were conducted so as to provide a reference in the context of the hot-corrosion studies. The commercial alloys examined under these conditions can be divided in two distinct groups with respect to the morphology, structure, and growth kinetics of the oxide scale. These two alloy groups will be designated as either Cr_2O_3-forming or Al_2O_3-forming. This distinction is, of course, well known and can be predicted to a certain extent from the Ni–Cr–Al ternary oxide scale diagram.[4] The important implications that the simple oxidation scale has on hot-corrosion behavior will be demonstrated in this study.

The internal and external scale formations found for the Cr_2O_3-forming alloys are summarized in Table II. The notation adopted in Table II is as follows: the scale compositions are from left to right as they appear from the outside surface, with the external oxidation above and the internal oxidation below the horizontal line. The percentage of each scale type refers

Table III. Scale Compositions for the Al_2O_3-Forming Alloys Oxidized at 1000°C for 24 hr

Alloy	Cr	Al	Ti	Complex oxide–Al_2O_3	Cr_2O_3[a]–Al_2O_3	TiO_2–Al_2O_3
IN713LC	11.4	6.3	0.8	15%	85%	
IN100	9.8	5.9	4.8	25%		75%
MARM002	9.0	5.5	1.7	10%	90%	

[a]Thin discontinuous layer.

to the amount of surface area. It is interesting to note that the scale types vary within a particular alloy as well as from alloy to alloy. The alloy IN738, for example, which is nominally Cr_2O_3-forming, shows localized zones of Al_2O_3 formation as illustrated in Fig. 1(c). This scale irregularity is due to the relatively low Cr content for this class of alloy and the alloying element inhomogeneities that develop during the casting operation.

The external scale formation reflects the relatively high concentration of Cr and Ti within this alloy group. One notes that the predominant Cr_2O_3 layer is always situated beneath an external layer of TiO_2 and sometimes "sandwiched" between two titanium oxide layers. The lower layer consists

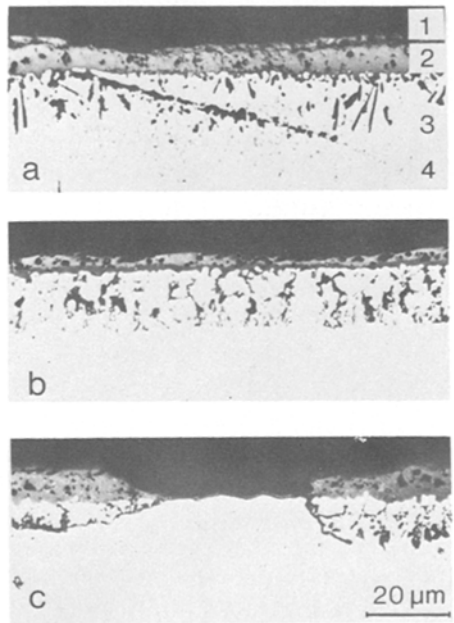

Fig. 1. Photomicrographs of the scales formed on the Cr_2O_3-forming alloys after simple oxidation for 24 hr at 1000°C. (a) IN597. 1, The external layer of TiO_2; 2, the underlying layer of Cr_2O_3; 3, the internally oxidized "fingers" of Al_2O_3; 4, the titanium-rich phase. (b) U710. Same scale as IN597 with the addition of a second titanium oxide layer between the Cr_2O_3 layer and the alloy substrate. Note that the external TiO_2 layer has been removed during polishing. (c) IN738. A localized transition from a Cr_2O_3-dominant scale to an Al_2O_3-dominant scale. No internal oxidation is associated with the Al_2O_3 scale.

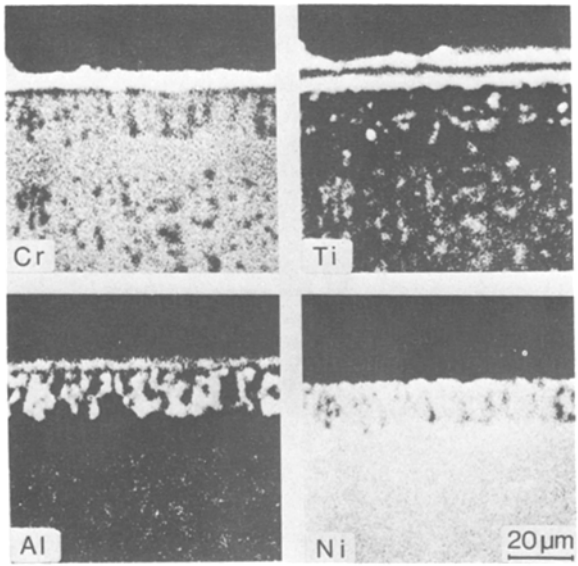

Fig. 2. X-ray images of U710 oxidized at 1000°C for 24 hr. The external scale consists of a layer of Cr_2O_3 "sandwiched" between two layers of titanium oxide, while the internal scale consists of Al_2O_3 "fingers" and titanium-rich particles.

probably of a suboxide of titanium. This structure is shown in Fig. 1(a) and (b) and is supported by the x-ray images in Fig. 2.

The ratio of the thickness of the subscale to that of the external scale increases with increasing temperature. The nature of the external scale dictates that the subscale is depleted in Cr and Ti while enriched in elements such as Ni, Co, Mo, and Al. This latter element is oxidized internally to form elongated particles or "fingers" of Al_2O_3.

The scale morphology of the Al_2O_3-forming alloys is characterized by the presence of a thin continuous layer of Al_2O_3 adjacent to the metal substrate, as shown in Fig. 3. The Al_2O_3 layer may be covered by a thicker external layer whose composition varies within any one alloy as well as from alloy to alloy. One notes as well the absence of an internal scale. The disposition of the scale products of the Al_2O_3-forming alloys is shown in Table III. An interesting point in this table is the occurrence of TiO_2 in the external layer of the IN100 alloy.

The oxidation kinetics of the two alloy classes are shown in Fig. 4. The higher oxidation rates of the Cr_2O_3-forming alloys with respect to those of the Al_2O_3-forming alloys simply reflect the fact that overall scale growth

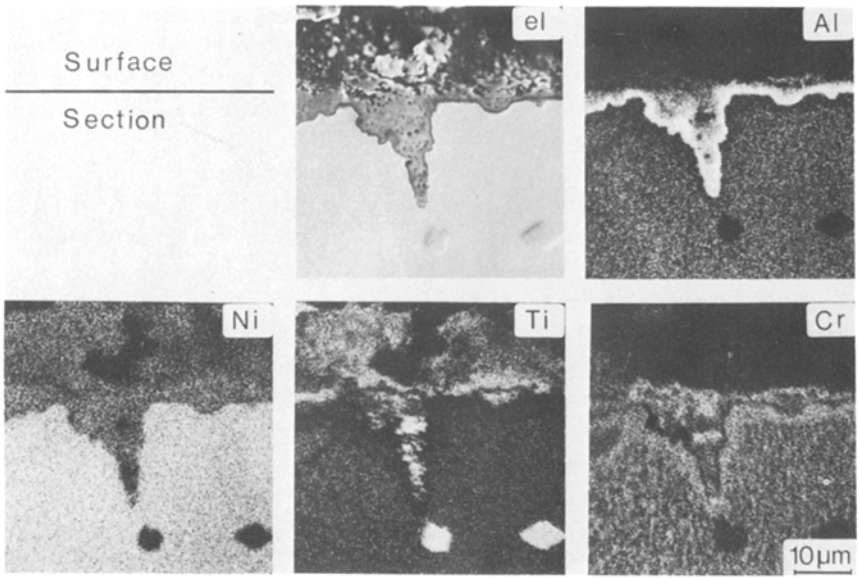

Fig. 3. Electron and x-ray images of IN100 oxidized at 1000°C for 24 hr, illustrating the continuous layer of Al_2O_3 situated between the metal substrate and the external layer of complex oxides. Note that the specimen is oriented so that both the section and the surface are visible.

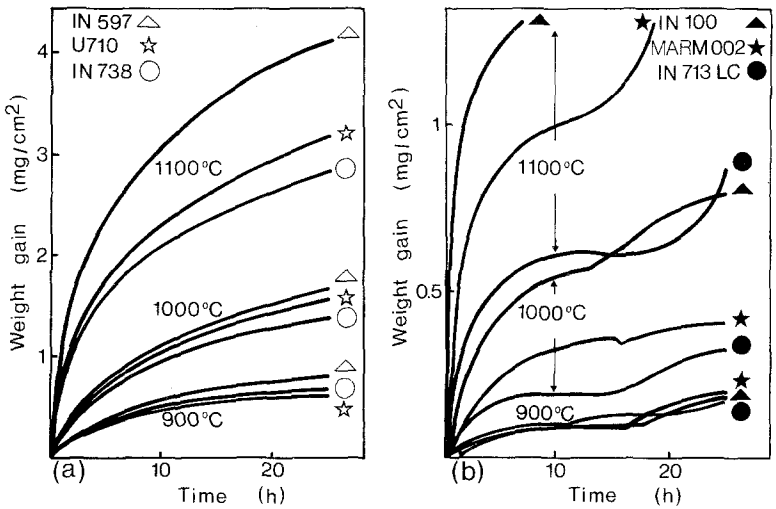

Fig. 4. Thermobalance curves for simple oxidation in still air. (a) Cr_2O_3-forming alloys; parabolic oxidation kinetics except for the initial hours. (b) Al_2O_3-forming alloys; nonparabolic oxidation kinetics with discontinuities.

is controlled, respectively, by these two oxides. The kinetics for the Cr_2O_3-forming alloys are parabolic, except for the initial several hours, and the rate constants compare well with those reported in the literature for this class of alloy.[4] The kinetics of the Al_2O_3-forming alloys do not follow a simple parabolic relationship. Instead, an initial rapid weight gain period is followed by an irregular plateau region that is often punctuated by discontinuities. The discontinuities in oxide growth rate are probably due to the marked tendency for the Al_2O_3-forming alloys to spall, which was noted during cooling from the test temperature.

The simple oxidation experiments described here are admittedly cursory in nature since they were designed to serve essentially as a base line reference for the hot-corrosion studies. As such, the results are not complete since, for example, the morphology, structure, and oxidation kinetics could evolve with oxidation time and temperature. Nevertheless, oxidation times up to 170 hr and oxidation temperatures of 900 and 1100°C showed essentially the same behavior as that described for the 24-hr trials at 1000°C. As will be seen in the following sections of this paper, the important point of the simple oxidation studies is the classification of the alloys into the two oxide scale categories, that is, Al_2O_3- and Cr_2O_3-forming.

Oxidation with Na_2SO_4

The effect of Na_2SO_4 on the oxidation kinetics and the morphology of the scale varied considerably according to whether the alloy was Cr_2O_3-forming or Al_2O_3-forming during simple oxidation. The details of hot corrosion due to Na_2SO_4 will, therefore, be discussed within each alloy class.

The Cr_2O_3-Forming Alloys

The oxidation kinetics and scale structures produced under hot-corrosion conditions for the Cr_2O_3-forming alloys were essentially the same as those reported for simple oxidation. This result was true for all the times and Na_2SO_4 coatings examined at 900°C. Also, thermal shocking during the test had no effect.

The only difference that was discerned with respect to the oxidation kinetics was the tendency for the hot-corrosion specimens to gain weight less rapidly during the first hours of the test than their simple oxidation counterparts. Weight losses were found in some cases. This phenomenon has been reported elsewhere[5] and is due to the formation of volatile sodium compounds, such as Na_2CrO_4.

The internal oxidation appeared to be accelerated slightly by the presence of a preceding internal sulfidation zone. The sulfides consisted principally of titanium and chromium.

The lack of susceptibility to Na_2SO_4-induced hot corrosion that was displayed by the Cr_2O_3-forming alloys depended on the existence of the protective Cr_2O_3 layer. As will be discussed in the next section, removal of this layer resulted in heavy corrosion for this class of alloys.

The Al_2O_3-Forming Alloys

As opposed to the Cr_2O_3-forming alloys, the Al_2O_3-forming alloys suffered extensive hot corrosion when oxidized in the presence of Na_2SO_4.

Figure 5(a) shows the thermogravimetric curves for the three Al_2O_3-forming alloys that resulted from a moderate deposit (0.5 mg/cm^2) of Na_2SO_4. The general form of these curves is characteristic in that the following distinct regions may be noted:

1. An initial incubation period, t_1, followed by a quasiparabolic oxidation region;
2. An inflection point, t_2, followed by a quasilinear oxidation region of approximately 2 mg/cm^2 hr;
3. A plateau region in the case of Na_2SO_4 deposits less than about 2 mg/cm^2. For larger repetitive amounts, the quasilinear region can continue until the specimen is completely oxidized [Fig. 5(b)].

The significance of the incubation period and the inflection point will be noted later in conjunction with the scale morphology. However, Arrhenius constructions for t_1 and t_2 (Fig. 6) show straight lines with no discontinuities at the melting point of Na_2SO_4 (884°C). The inflection point was also found to be influenced by the importance of the Na_2SO_4 deposit. Amounts greater or less than about 0.5 mg/cm^2 increased t_2 while not changing significantly the quantity of scale accumulated at the inflection point.

Slow thermal cycling of specimens in the plateau region did not alter the oxidation kinetics. Repetitive contamination, on the other hand reactivated the linear regime.

Surface treatments that alter the alloy composition in the near-surface volume can affect hot-corrosion behavior considerably. A simple preoxidation of the IN713LC alloy followed by a hot-corrosion trial effectively decreased the weight gain during the initial parabolic region but not during the linear regime [Fig. 5(b)]. Perhaps more important was the fact that U710, which was shown to be insensitive to Na_2SO_4, was made to suffer hot corrosion by preoxidizing and subsequently mechanically abrading the resultant Cr_2O_3 layer before the hot-corrosion trial. This phenomenon is shown in Fig. 5(a) with the curve for U710 designated with a star (☆).

The MARM002 alloy proved to be generally more resistant to hot corrosion than the other two Al_2O_3-forming alloys. This superiority was most marked in the case of heavy contaminations (1 to 2 mg/cm^2) where the oxidation kinetics for MARM002 appeared to be distinctly different

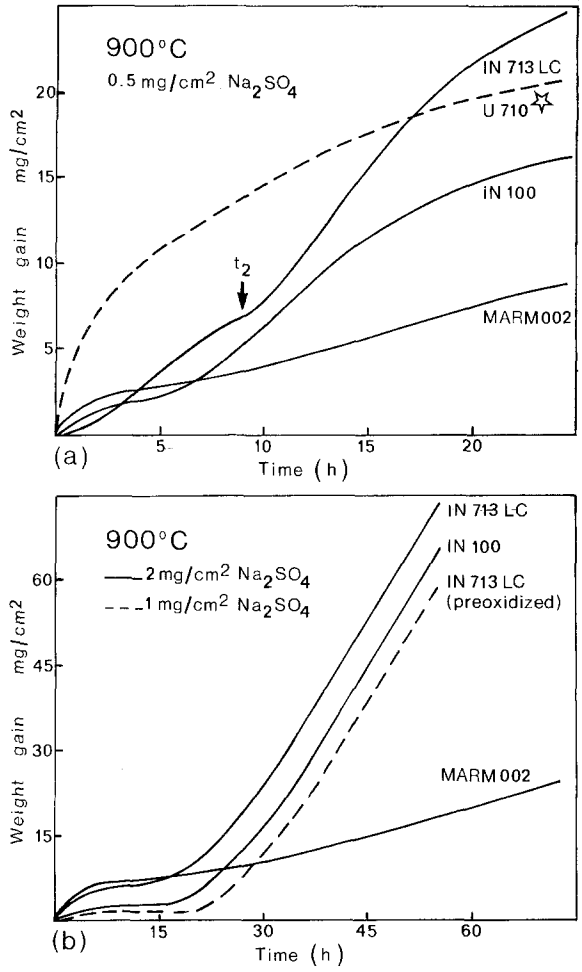

Fig. 5. Thermobalance curves for hot corrosion of the Al_2O_3-forming alloys with Na_2SO_4. (a) Moderate contamination. Four distinct regions are evident—an initial incubation period, a quasiparabolic region, a quasilinear region starting at t_2, and a plateau region. (b) Heavy contamination. The linear region is extended. Note that preoxidation suppresses the parabolic region only.

during the linear regime. No distinction could be made, however, for very heavy repetitive contamination (about 5 mg/cm^2 for each dose).

The hot-corrosion scale morphology and structure of the Al_2O_3-forming alloys depended on the quantity of contamination and whether the specimen was in the quasiparabolic, the quasilinear, or the plateau region.

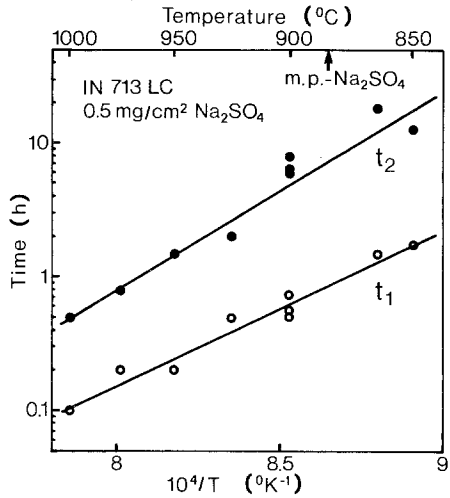

Fig. 6. Arrhenius constructions of the incubation time, t_1, and the inflection point, t_2, produce straight lines with no discontinuities at the melting point of Na_2SO_4.

One finds, as well, certain fundamental differences within this alloy class that appear to be related to the quantity and nature of the refractory element additions, such as molybdenum, vanadium, and tungsten.

The scale morphology and structure of the molybdenum- and vanadium-bearing alloys (IN713LC and IN100) were quite different from those of the tungsten-bearing alloy (MARM002) for hot corrosion with moderate to heavy Na_2SO_4 deposits (0.5 to 2 mg/cm^2). A corresponding difference in the oxidation kinetics has already been described. Further, only the molybdenum- and vanadium-bearing alloys experienced heavy spalling during rapid cooling from the test temperature. The external scale was ejected from the substrate as a whole.

The hot-corrosion scale produced on the molybdenum- and vanadium-bearing alloys changed radically during the transition from the quasi-parabolic to the quasilinear regions of the thermogravimetric curve. During the former regime, a compact layered scale grew uniformly throughout the specimen surface. The initiation of the linear regime coincided with the nonuniform formation of a thick porous scale. The porous scale initiated at the specimen edges and progressed laterally across the specimen surface. This process was exemplified by the preoxidized specimen shown in Fig. 7. The plateau region was attained when the heterogeneous corrosion process had completely consumed the specimen surface. The penetration of the attack toward the core of the specimen was eventually stopped by the

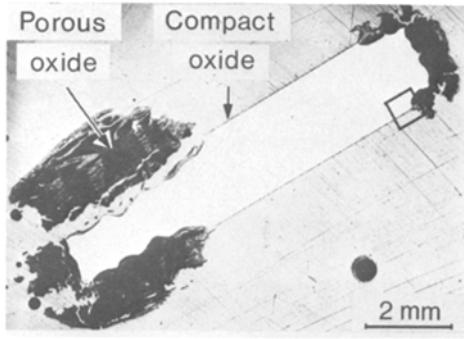

Fig. 7. Macrographic section of a molybdenum-bearing Al_2O_3-forming alloy that has attained the linear region of the hot corrosion curve. The lateral propagation of the porous–compact scale interface is evident (IN713LC preoxidized, subsequently oxidized at 900°C with 1 mg/cm^2 Na_2SO_4).

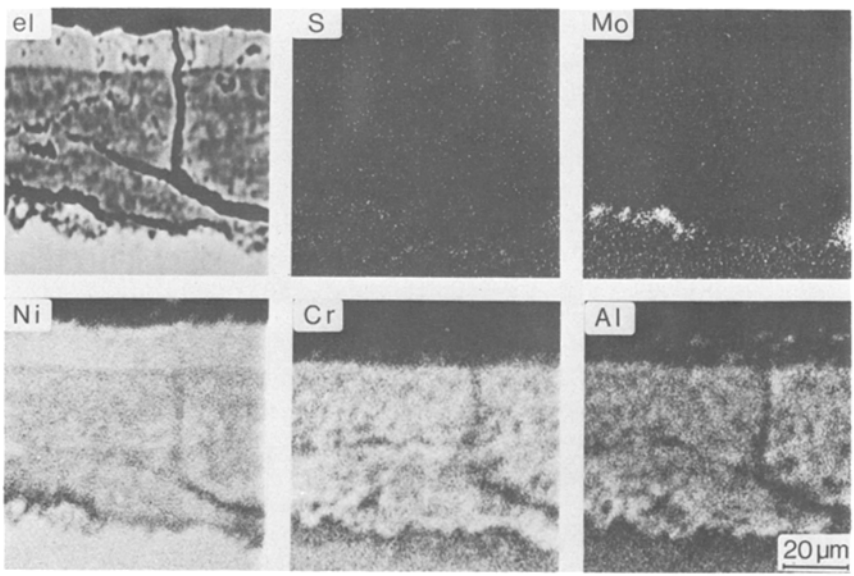

Fig. 8. Electron and x-ray images of the compact scale corresponding to the quasiparabolic region of the hot-corrosion curve. The compact scale, while fissured, is adherent to the substrate (IN713LC oxidized for 8 hr at 900°C with 0.5 mg/cm^2 Na_2SO_4).

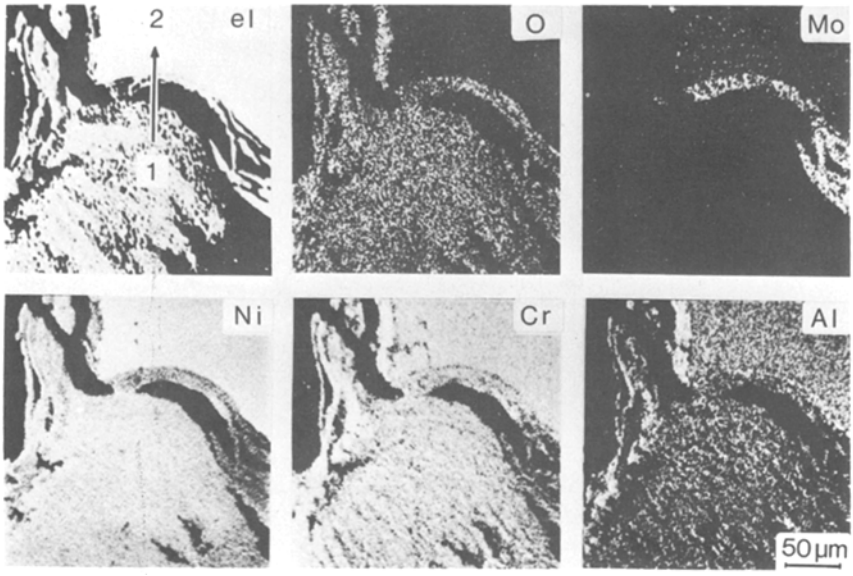

Fig. 9. Electron and x-ray images of the laterally propagating interface contained within the area outlined by the square in Fig. 7. The arrow indicates the growth direction of the porous scale (1) into the compact-scale-covered substrate (2). The porous scale has spalled at the molybdenum-rich phase.

reformation of a compact oxide between the porous scale and the metal substrate.

Figure 8 shows electron and x-ray images of the scale corresponding to the quasiparabolic regime. The stratified scale is composed of external layers of an oxide of niobium and NiO with an underlying layer of a mixture of oxides, principally NiO and $Ni(Cr,Al)_2O_4$. Sulfur has penetrated into the subscale while molybdenum has accumulated immediately beneath the external scale.

The chemical composition of the propagating interface situated between the compact and the porous oxide regions is shown in the x-ray images of Fig. 9. The important point to note is the presence of a molybdenum-rich oxide layer that separates the metal substrate and the unstratified porous scale. Although the refractory elements are not present in the porous scale, the other alloy elements, such as Ni, Cr, Al, Ti, and Nb, appear to have been oxidized without preference. The porous scale consists of a mixture of the same oxides contained in the compact scale but in different proportions. Figure 10(a) and (b) show, respectively, the results of electron microprobe scans effected across the molybdenum-rich layers of IN713LC and IN100. In both cases, the molybdenum concentration is about an order of magnitude

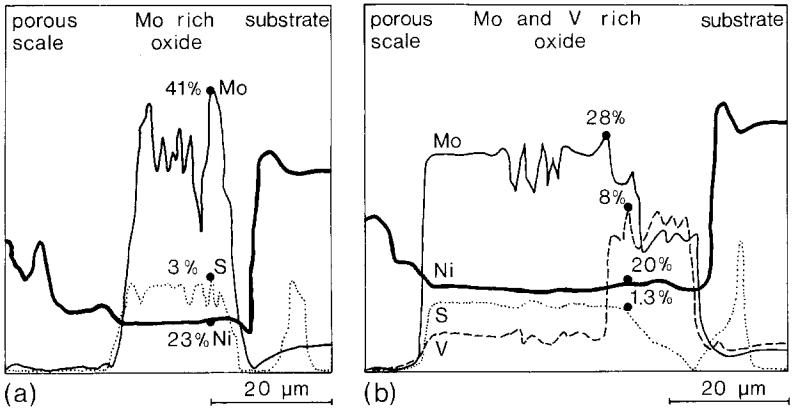

Fig. 10. Electron microprobe scans of the refractory element layers separating the substrate and the porous oxide scale. (a) IN713LC; molybdenum-bearing. (b) IN100; molybdenum- and vanadium-bearing (oxidized for 60 hr at 900°C with 2 mg/cm^2 Na_2SO_4).

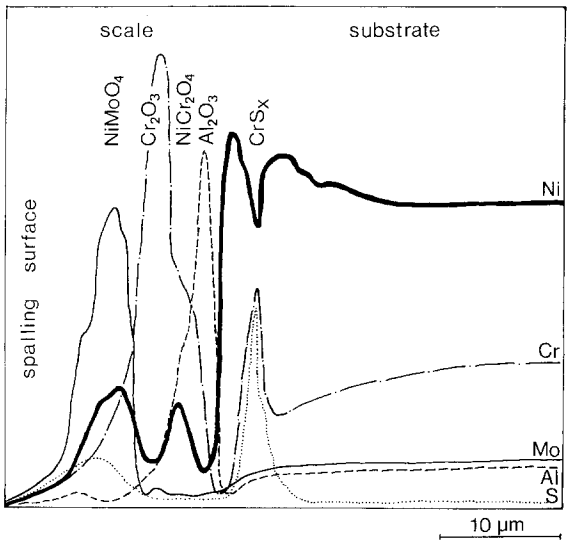

Fig. 11. Electron microprobe scan of the compact scale adherent to the substrate. The spalling surface is coincident with the $NiMoO_4$ layer (IN713LC oxidized for 48 hr at 900°C with 0.5 mg/cm^2 Na_2SO_4).

greater than that contained globally in the alloy. The vanadium-containing alloy, IN100, has produced two refractory-element-rich layers, an external layer containing principally molybdenum and an internal layer containing both molybdenum and vanadium. The vandium concentration has also increased to about an order of magnitude over that in the alloy. Sulfur has accumulated within the refractory element layers as well as in the metal substrate adjacent to these layers.

The plateau region of the hot-corrosion curve is attained when the porous oxide has completely enveloped the specimen. The penetration of the attack toward the core of the specimen is stopped by the formation of a compact scale next to the substrate, as shown in Fig. 11. This scale consists of successive layers of Cr_2O_3, $NiCr_2O_4$, and Al_2O_3. The molybdenum-rich layer, present during the linear regime, has been transformed into $NiMoO_4$. The spalling surface generated during cooling is coincident with the $NiMoO_4$ layer.

The tungsten-bearing alloy, MARM002, produced only a compact scale during hot corrosion with moderate to heavy deposits of Na_2SO_4. The morphology and chemical composition of this scale are shown in the electron and x-ray images of Fig. 12. The scale was stratified and, from the

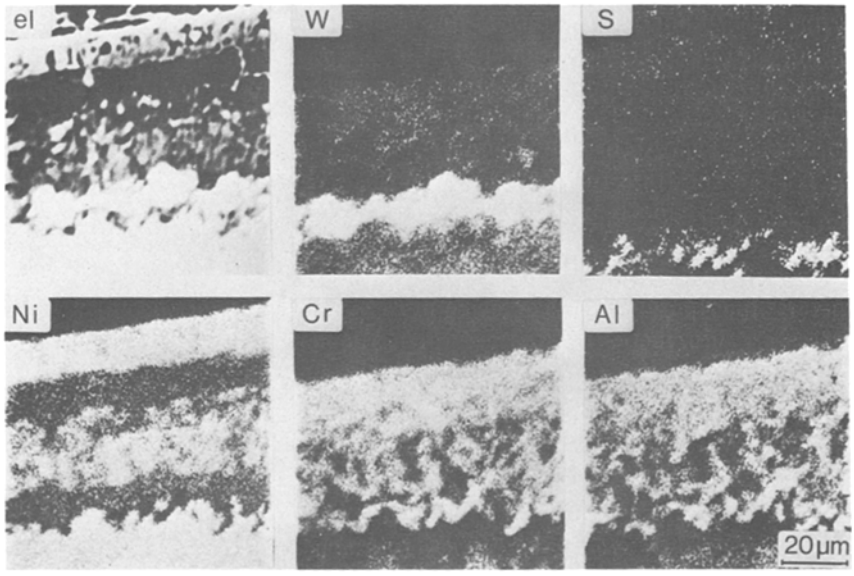

Fig. 12. Electron and x-ray images of the compact scale formed on the tungsten-bearing alloy (MARM002 oxidized for 24 hr at 900°C with 0.5 mg/cm^2 Na_2SO_4).

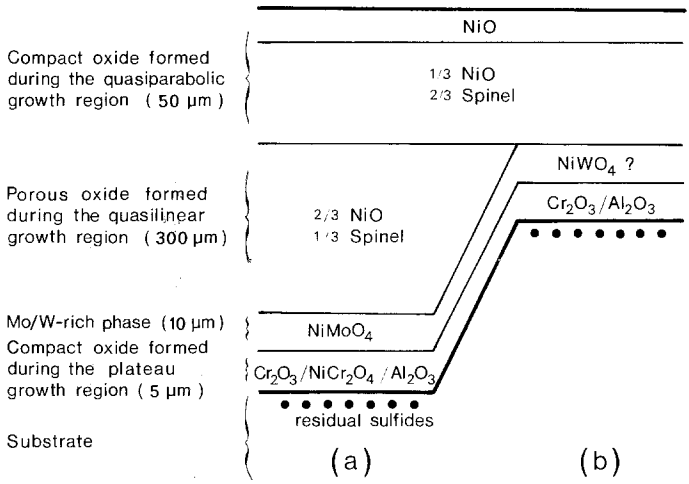

Fig. 13. Schematic summary of the hot-corrosion scales attained in the plateau region by the Al_2O_3-forming alloys oxidized with moderate to heavy Na_2SO_4 contamination. (a) The molybdenum or molybdenum- and vanadium-bearing alloys (IN713LC and IN100). (b) The tungsten-bearing alloy (MARM002).

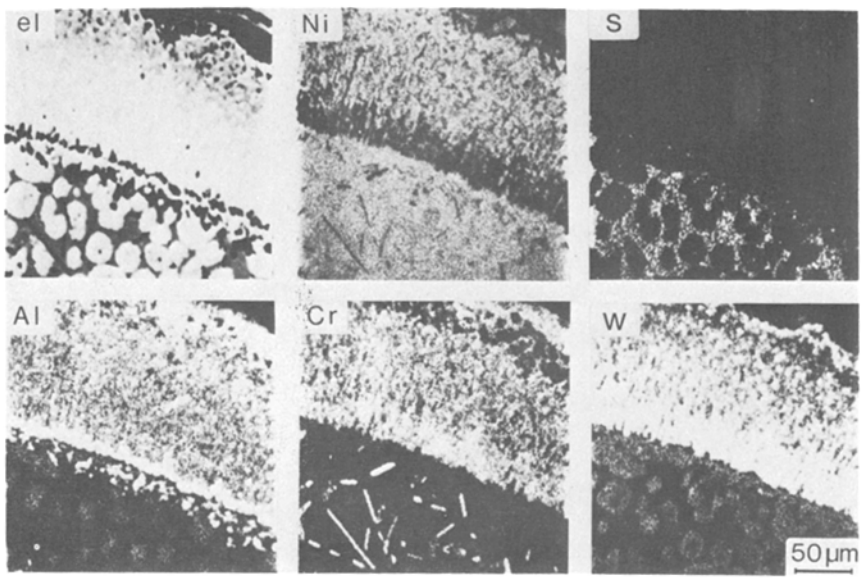

Fig. 14. Electron and x-ray images of the scale formed on alloy MARM002 after oxidation for 100 hr at 900°C with very heavy (about 5 mg/cm^2) repetitive depositions of Na_2SO_4. A continuous internal network of the eutectic Ni–Ni_3S_2 precedes oxidation.

outside layer, consisted of (Ni,Co)O, $(Ni,Co)(Al,Cr)_2O_4$, probably $NiWO_4$, Cr_2O_3, and Al_2O_3. Sulfur was concentrated in the subscale, while tantalum was present in the spinel layer of the scale. Hafnium appeared to be uniformly distributed throughout the substrate and scale, except for the (Ni,Co)O layer.

The disposition and composition of the layers composing the hot-corrosion scales attained in the plateau region for moderate to heavy Na_2SO_4 contamination are summarized schematically in Fig. 13.

As noted previously, no distinction could be made between the three Al_2O_3-forming alloys, as far as the scale growth kinetics were concerned, in the case of hot corrosion with renewed very heavy Na_2SO_4 deposits (approximately 5 mg/cm^2). The similarity in kinetics for these severe conditions was reflected by the similitude in scale morphology for all three alloys.

The essential characteristic of hot corrosion with very heavy contamination was the extensive sulfide formation in the substrate, adjacent to the oxide scale. As shown in Fig. 14, the sulfide networks preceded the oxide scale and extended approximately 100 μm into the substrate. The principal sulfide phase in the case of MARM002 was identified as the eutectic Ni–Ni_3S_2, whereas Cr_2S_3 appeared predominantly in the IN713LC alloy. On the other hand, IN100 showed evidence of a molybdenum-containing Na_2SO_4 phase lying between the scale and the substrate. This was the only occasion where Na_2SO_4 was identified in the hot-corrosion scale.

Oxidation with NaCl

Thermogravimetric curves for hot corrosion at 900°C with a 0.5 mg/cm^2 deposit of NaCl are shown in Fig. 15. Contrary to the results obtained with Na_2SO_4 contamination, the Cr_2O_3-forming alloys were susceptible to hot corrosion with NaCl, while the Al_2O_3-forming alloys were relatively insensitive to attack. Alloy IN100 is a notable exception to this generalization. In addition, hot corrosion with NaCl was also less intense than that found for Na_2SO_4. Further, the form of the thermogravimetric curves did not obey a simple growth law. After an initial rapid weight gain period, a subsequent quasilinear growth regime was established. The quasilinear regime extended unchanged up to the longest test times, approximately 50 hr.

In the case of Na_2SO_4 contamination, a protective Cr_2O_3-forming alloy (U710) was rendered susceptible to hot corrosion by preoxidizing and mechanically removing the resultant oxide. The reverse was true for NaCl contamination in that the same surface treatment transformed the highly susceptible alloy U710 into an insensitive one (Fig. 15). A similar result was also obtained by simply preoxidizing the alloy.

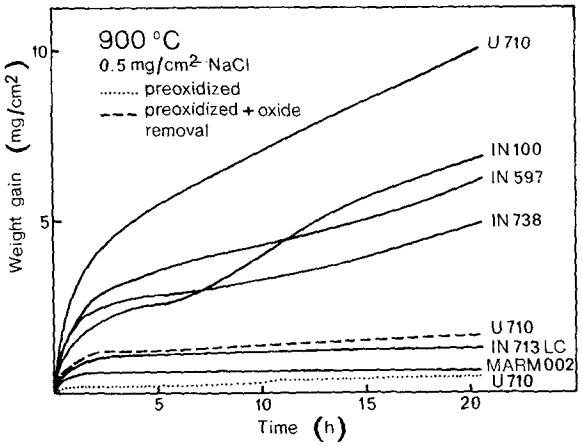

Fig. 15. Thermobalance curves for hot corrosion with NaCl.

Figure 16 shows the morphology and chemical composition of the scale formed on U710 after hot corrosion with NaCl. Starting from the outermost layer, the structure of the detached scale was determined to be (Ni,Co)O, TiO_2, possibly $(Cr,Al)_2O_3$, and a titanium-rich layer that appears

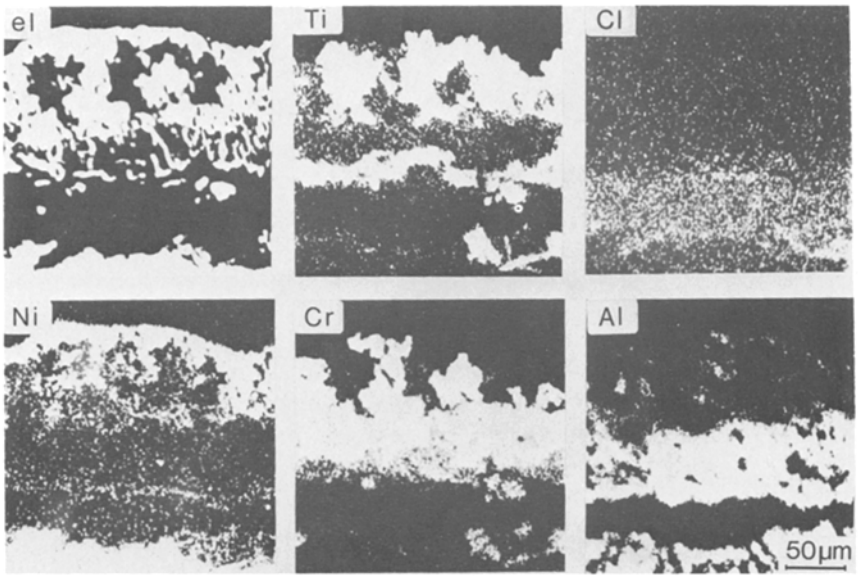

Fig. 16. Electron and x-ray images of the scale formed on alloy U710 after oxidation for 24 hr at 900°C with 0.5 mg/cm² NaCl. The scale has spalled from the substrate.

to be associated with chlorine. Separation occurred within this last layer. No trace of sodium was detected. The subscale was composed principally of Al_2O_3 "fingers."

IN100, the only Al_2O_3-forming alloy found susceptible to NaCl, produced a scale covered by nodule-like growths. Here again, an association was found between titanium and chlorine, particularly in the nodules.

Oxidation with a 10:1 Mixture of Na_2SO_4 and NaCl

The oxidation trials with pure NaCl being only academic as far as gas turbine conditions are concerned, a series of experiments were carried out at 900°C with a 10:1 mixture of Na_2SO_4 and NaCl, respectively.

As reported earlier, the Al_2O_3-forming alloys suffered accelerated or catastrophic hot corrosion in the presence of a Na_2SO_4 coating. The addition of a small amount of NaCl to the Na_2SO_4 deposit (10:1 Na_2SO_4 to NaCl by weight for a total deposit of 0.55 mg/cm^2) provoked a contraction in the time scale of the curves established for oxidation with pure Na_2SO_4. The weight gains attained in the plateau region of the curves were slightly increased by the presence of NaCl. The scale compositions and morphologies were essentially the same as those obtained with pure Na_2SO_4.

The oxidation kinetics and scale compositions pertaining to the Cr_2O_3-forming alloys oxidized with the salt mixture depended on the total salt weight applied. In the case of moderate contamination (0.55 mg/cm^2), the presence of NaCl changed neither the oxidation kinetics nor the scale composition from that obtained with only Na_2SO_4. However, the salt mixture did cause heavy spalling during cooling from the test temperature.

On the other hand, very heavy salt mixture contamination (5.5 mg/cm^2) did provoke hot corrosion of the Cr_2O_3-forming alloys. The Cr_2O_3 layer, predominant for simple oxidation and oxidation with Na_2SO_4 alone, was transformed to $Ni(Cr,Al)_2O_4$ in the case of the salt mixture. Further, the internal scaling was increased to a depth of about 100 μm. However, as opposed to moderate salt mixture contamination, no spalling was observed during cooling.

SUMMARY

An important result of this investigation was the relationship established between hot-corrosion susceptibility and the composition of the scale formed during simple oxidation.

In the case of Na_2SO_4 contamination, the immunity of the alloys under consideration was not found to be related to the chromium content in a monotonic manner. The critical factor for protection was the ability of the alloy to form a continuous layer of Cr_2O_3 during simple oxidation.

This point is illustrated by the fact that, among the susceptible Al_2O_3-forming alloys, IN713LC has the highest chromium content but the worst hot-corrosion performance. Also, within the nonsusceptible Cr_2O_3-forming group, IN597, a high chromium content alloy, does not appear to offer any advantage over IN738, which has the lowest chromium content of this group. In this last case, however, an advantage may be evident for hot-corrosion tests of much larger duration than those employed in this study.

Susceptibility to hot corrosion with NaCl alone appears to be related to the formation of Cr_2O_3 or TiO_2 or both during simple oxidation. As far as Cr_2O_3 is concerned, this behavior is the reverse of that found for Na_2SO_4 contamination. Again, the hot-corrosion phenomenon has an "all or nothing" aspect in that, within the susceptible alloy group, no monotonic correlation is evident between hot-corrosion severity and chromium or titanium content.

The nature of the hot-corrosion attack with Na_2SO_4 appeared to offer more ramifications than those found for NaCl. Three distinct, but sometimes sequential, hot-corrosion types were established for Na_2SO_4 contamination. Their occurrence depended principally on the quantity of contaminant. All of these hot-corrosion types have been reported previously in the literature and have given rise to at least an equal number of mechanistic theories. The practical importance of any particular mechanism depends, of course, on whether the corresponding laboratory-produced hot-corrosion morphology is identified with that produced with operating gas turbine conditions.

Very heavy repetitive Na_2SO_4 deposits provoked catastrophic linear oxidation that appeared frequently to be related to liquid phase attack. The corrosive liquids were either low-melting-point sulfides, such as the Ni–Ni_3S_2 eutectic (melting point of 637°C), or refractory-element-bearing Na_2SO_4. The hot-corrosion kinetics under these conditions are rapid and linear since the reaction rate between the liquid phase and the metal substrate is interfacially controlled. In the case of liquid sulfide, the attack is that of sulfidation followed by oxidation.[6–8] The flux theory[9] is applicable to direct corrosion by the sulfate phase. According to this theory, the Na_2SO_4 acts as either a basic or an acidic flux for the oxide scale depending on the quantity and type of dissolved elements, notably the refractory elements. However, no differentiation was evident in this study, as far as hot-corrosion kinetics were concerned, among the susceptible alloys tested with very heavy Na_2SO_4 deposits.

A sequential attack was found to be operative for Na_2SO_4 deposits less than that necessary to form liquid sulfide networks. That is, after an initial incubation period, two distinct hot-corrosion processes intervened sequentially and corresponded to the quasiparabolic and the quasilinear regimes of the thermogravimetric curves. The morphology corresponding

to the quasiparabolic regime was that of a layered compact oxide, overlying internal sulfidation. This situation is similar to that described before,[8,10,11] where sulfur diffuses rapidly into the substrate and effectively decreases the chromium activity through sulfide formation. In addition, this study found that the refractory elements (molybdenum, vanadium, and tungsten) were concentrated at the scale–substrate interface during the quasiparabolic stage. The initiation of the quasilinear regime was coincident with the transformation of this refractory element zone into a distinct phase. However, the rapid linear oxidation kinetics and the accompanying porous scale were associated only with the molybdenum or with the molybdenum- and vanadium-bearing alloys. The tungsten-bearing alloy was much more resistant and formed a compact scale. Brenner[12] has shown in the case of Fe–Ni–Mo and Fe–Cr–Mo alloys that catastrophic oxidation can ensue when the low-melting-point (795°C) phase, MoO_3, is formed. The melting point of this phase can be lowered to approximately 760°C[13] upon the dissolution of certain elements, such as nickel or chromium. The linear oxidation kinetics associated with this attack were proposed to be due to the dissolution of the substrate elements into the liquid MoO_3 phase and their subsequent oxidation at the scale–liquid phase interface. According to the results of the present study, this process described by Brenner appears to be operative in nickel-base superalloys as well. One notes that the melting point of WO_3 (1470°C) is much higher than the test temperatures employed in this study. The eventual formation of $NiMoO_4$ will stop the liquid phase attack since the melting point for this compound is high (1350°C). $NiMoO_4$ was identified between the porous scale and the underlying compact scale. The cause of the heavy spalling during cooling is due to allotropic transformations within the $NiMoO_4$ phase.[14]

The accelerated attack during the quasiparabolic regime, due to the action of internal sulfidation, would appear to prepare the conditions necessary for the formation of a refractory element liquid phase. The liquid phase, once formed between the compact oxide scale and the substrate, produces catastrophic attack until solid $NiMoO_4$ is established. The linear regime can be reactivated by an additional Na_2SO_4 deposition. The verification of this mechanism in detail is the object of an ongoing study.

The results found for hot corrosion with NaCl alone appear to support the theory proposed by Condé[15] and by Hancock.[16] Their theory suggests that the formation of volatile oxychlorides between the scale and the substrate will result in the mechanical degradation of the former. The present study has established a correlation between the presence of titanium and chromium (both volatile oxychloride formers) in the scale and hot-corrosion susceptibility. This correlation was reinforced by the lack of attack evident on Cr_2O_3-forming specimens that were previously depeleted superficially

in chromium and titanium with a preoxidation and abrasion treatment. Chlorine was also found at the scale–substrate interface. Under more realistic conditions, such as small concentrations of NaCl in Na_2SO_4 deposits, the principal role of NaCl is to promote the thermal-cycling-induced spalling of the Na_2SO_4 protective layer that is indigenous to the Cr_2O_3-forming alloys. This report has demonstrated that the removal of this protective oxide layer can lead to Na_2SO_4 attack that is equal in importance to that found for the Al_2O_3-forming alloys.

ACKNOWLEDGMENTS

The authors wish to express their appreciation for the alloys supplied by the Société Nationale d'Etude et de Construction de Moteurs d'Aviation.

REFERENCES

1. C. T. Sims, P. A. Bergman, and A. M. Beltran, ASME Paper No. 69-GT-16 (March 1969).
2. R. Morbioli, S. Ferre, and R. Brunetaud, SNECMA Internal Report YORC No. 41.741 (1974).
3. M. Tong, *J. Microsc. (Paris)* **8**, 269–306 (1969).
4. G. W. Goward, *J. Met.* **22**, 31 (1970).
5. N. S. Bornstein and M. A. DeCrescente, *Metall. Trans.* **2**, 2875 (1971).
6. E. L. Simons, G. V. Browning, and M. A. Liebhafsky, *Corrosion* **11**, 505t (1955).
7. A. U. Seybolt, General Electric Internal Report No. 70-C-189 (1970).
8. M. E. El-Dashan, D. P. Whittle, and J. Stringer, *Oxid. Met.* **8**, 179 (1974).
9. J. A. Goebel, F. S. Pettit, and G. W. Goward, *Metall. Trans.* **4**, 261 (1973).
10. C. J. Spengler and R. Viswanathan, *Metall. Trans.* **3**, 161 (1972).
11. G. J. Danek, Jr., *Nav. Eng. J.* 77, 859 (1965).
12. S. S. Brenner, *J. Electrochem. Soc.* **102**, 16 (1955).
13. G. W. Rathenau and J. L. Meijering, *Metallurgia* **42**, 167 (1950).
14. S. S. Brenner, *J. Electrochem. Soc.* **102**, 7 (1955).
15. J. F. G. Condé, AGARD Conference, Copenhagen (1972).
16. R. C. Hurst, J. B. Johnson, M. Davies, and P. Hancock, C.E.G.B. Conference, London (1972).